

Behavior of charged and uncharged drops in high alternating tangential electric fieldsJens-Michael Löwe¹* and Volker Hinrichsen¹*High-Voltage Laboratories, Technische Universität Darmstadt, Darmstadt 64283, Germany*Iliia V. Roisman and Cameron Tropea¹*Institute of Fluid Mechanics and Aerodynamics, Technische Universität Darmstadt, Darmstadt 64283, Germany*

(Received 23 October 2019; accepted 7 January 2020; published 4 February 2020)

The interaction of drops and electric fields occurs in many applications like electrowetting, electrospinning, atomization, but also causes unwanted effects like the aging of high-voltage composite insulators. Water drops are influenced by electric fields due to the polar properties of the water molecules. The behavior of the drops depends on several parameters like the orientation and strength of the electric field, drop volume, and frequency of the applied field. In addition, electric charges can influence the behavior of drops significantly. However, the impact of electric charges, including the interaction with the drop as well as the electric field strength, is far from being well understood. In this work, the impact of electric charges on the behavior of single sessile drops is investigated experimentally under well-defined conditions. The effects of the drop volume, electric field strength, field frequency, and electric charge of the drop are studied. The necessary amount of charge to change the behavior of drops, depending on the applied electric field and drop volume, is determined and different drop behavior regimes are identified. Depending on the boundary conditions, the drop oscillates with the same or double the frequency of the applied voltage. The different regimes are investigated for the first three oscillation modes. The obtained results will help to improve the understanding and to manipulate the behavior of uncharged and charged drops in strong electric fields.

DOI: [10.1103/PhysRevE.101.023102](https://doi.org/10.1103/PhysRevE.101.023102)**I. INTRODUCTION**

The behavior of liquid drops, especially of water, inside electric fields was intensively investigated in the past [1–4]. Several authors investigated the impact of electric fields on drop movement and deformation depending on the electric field strength and field orientation because of their inherent great scientific interest and many applications, like electrowetting [5–7], electrospinning [8,9], laboratory-on-chip-devices [10–12], atomization [13,14], or aging of high-voltage equipment like composite insulators [15,16]. In high-voltage technology, the aging of outdoor composite insulators due to sessile drops is an issue to ensure a reliable and safe power transmission and distribution.

In several experimental and numerical investigations, the behavior of sessile drops in electric fields was determined [17–19]. Alternating electric fields lead to an oscillation of the drop depending on the frequency and the orientation of the electric field and may lead to resonance of the drop, resulting in drop movement for large amplitudes and electric field strength [17,20]. In contrast, constant electric fields cause a deformation of the drop and can also lead to drop movement [21,22]. In addition to the mechanical deformation or oscillation of the drop, a sessile drop creates electrical critical points due to the field enhancement directly at the three-phase contact line. As a consequence, partial discharges may occur,

which deteriorate the surface of the substrate and enhance the aging process. Sessile drops on the surface of high-voltage insulators are exposed to an electric field with components normally and tangentially aligned to the substrate's surface. Both components of the electric field have an impact on the drop. Nevertheless, the component tangential to the substrate has a higher impact on the motion and oscillation of the drop [23] and, it is therefore more critical with respect to partial discharges and surface degradation.

Although the general behavior of drops in electric fields is known, the influence of electric charges on the behavior of sessile drops in alternating electric fields tangentially aligned to the substrate is still not completely understood. Several theories aim to predict the behavior of charged drops without quantifying the amount of charge and the interaction between the electric charge and the electric field strength [24,25].

Already small amounts of charge can influence the behavior of drops significantly, for example, during substrate-drop interaction [26]. Depending on the surface charge distribution on the substrate, charges can be transferred from the substrate to the drop or vice versa [27], so that a very careful handling of the drops and the substrate's surface is necessary. Especially, the use of conventional pipettes, which are widely used in laboratories, can lead to unwanted charges on drops [28]. Most of the previously investigated sessile drops on insulating substrates are unintentionally charged due to drop-substrate interaction or charged rain [29–31]. Consequently, it can be assumed that most of the performed experiments in literature have used charged drops with an unknown amount of charge.

*loewe@hst.tu-darmstadt.de

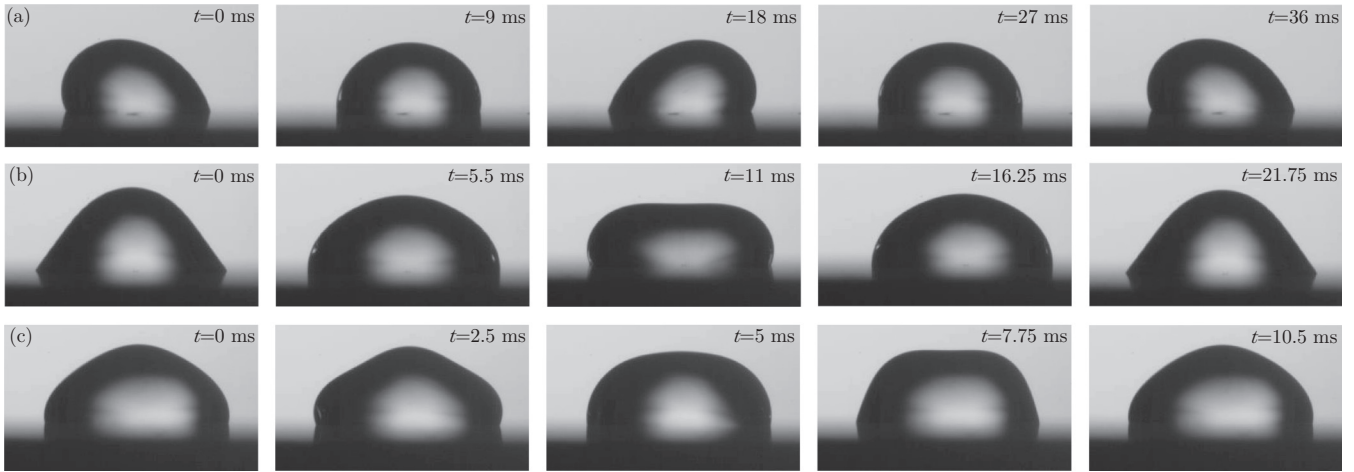


FIG. 1. One cycle of the first three modes for $n = 2, 3, 4$ of uncharged drops. (a) Example of mode 1 ($n = 2$) of a $20\text{-}\mu\text{l}$ drop at 27 Hz and $\hat{E} = 3.81\text{ kV/cm}$, (b) example of mode 2 ($n = 3$) of a $30\text{-}\mu\text{l}$ drop at 23 Hz and $\hat{E} = 4.67\text{ kV/cm}$, and (c) example of mode 3 ($n = 4$) of a $60\text{-}\mu\text{l}$ drop at 48 Hz and $\hat{E} = 7.37\text{ kV/cm}$. The videos can be found in the Supplemental Material [35].

The shape of sessile drops is defined by surface tension, gravity, as well as the substrate properties. The Bond number

$$\text{Bo} = \rho g d^2 / \gamma \quad (1)$$

characterizes the ratio of the force due to surface tension γ and gravity g and includes the drop diameter d and the density ρ of the drop. This study includes drops with $O(\text{Bo}) = 1$ so that gravity and surface tension both determine the drop shape. The surface tension tries to minimize the surface energy, resulting in an equilibrium shape, which is determined by a balance of the interfacial stresses. External forces caused by pressure fluctuations, fluid flow, or electric fields may lead to a deformation of the drop. Especially, a periodic force leads to a periodic deformation of the drop. The drop itself is an oscillatory system with characteristic resonance frequencies [32–34]. In case of a liquid (water) drop surrounded by liquid with much smaller density (air) and neglecting the effect of viscosity under the impact of an electric field, the excitation frequencies f for resonance are given by the following simplified expression [17,33]:

$$f = \left[\frac{n(n-1)(n+2)\gamma}{12V\pi\rho} \right]^{1/2} \quad \text{for } n \geq 2, \quad (2)$$

where V is the drop volume and n is an integer corresponding to the different modes. It is noteworthy that Eq. (2) is only valid for small oscillations; hence, for limited electric field strengths. For large electric field strengths, the drop begins to move on the substrate, which is no longer captured by the model. The characteristic mode number is given by $n - 1$, due to the fact that a drop oscillating with $n = 1$ is not stable. Consequently, $n = 2$ corresponds to the first resonance mode. The charge of the drop can influence the stability of the oscillation and might lead to instabilities [1]. In this study, the charge applied on the drops is small enough and does not cause any instabilities. It is noteworthy that the resonance frequencies of sessile drops on hydrophobic substrates are the same as for free drops [17].

However, additional resonance frequencies appear due to the different boundary conditions, in particular the broken symmetry caused by the substrate [17]. Figure 1 shows the principal movement of the drop in resonance for the first three modes. Higher modes are comparable to the third resonance mode but have an increased number of steady nodes on the surface during the oscillation. Hence, it is assumed that the behavior of higher modes is similar to the third mode and is not further investigated in this study.

The movement, oscillation, or deformation of the drop inside the electric field is caused by different forces acting on the drop. The origin of the force is given by the Lorentz force. In the case of an uncharged drop and neglecting the influence of any magnetic fields, only the electric field causes a force on the drop, which is given by the dielectric and the electrostrictive forces and can be written as

$$f_e = -\frac{1}{2}E^2\nabla\epsilon + \nabla\left[\frac{1}{2}\epsilon\left(\frac{\rho}{\epsilon}\right)\left(\frac{\partial\epsilon}{\partial\rho}\right)_T E^2\right], \quad (3)$$

where ϵ is the product of the vacuum permittivity ϵ_0 and the relative permittivity ϵ_r , ∇ is the nabla operator, and E is the electric field strength, that is defined as $E = \hat{E} \sin(\omega t)$ [36]. It is noteworthy that f_e is a volume force. The force results from the highly polarized water molecules and the interaction of the dipole molecules with the electric field and is also called Kelvin polarization force. The dipoles are aligned because of the electric field. On the other hand, the electric relaxation time for the liquid has to be taken into account. The used liquid can be assumed as a perfect conductor or dielectric depending on the electric relaxation time. For water, the electric relaxation time is $O(\tau = \epsilon/\gamma_{el}) \approx 10^{-6} \dots 10^{-4}\text{ s}$ and, therefore, the liquid can be assumed as perfect conductor for the tested frequencies. In case of a perfect conductor, all net charges are located at the drop's interface and the electric field inside the drop vanishes [37]. Hence, the electric field (field lines) is normally aligned to the drop interface (equipotential surface) even if the undisturbed electric field without a drop is tangentially aligned to the substrate. Nevertheless, a nonhomogeneous electric field, as given in this study due to the experimental setup, leads to a net force resulting from

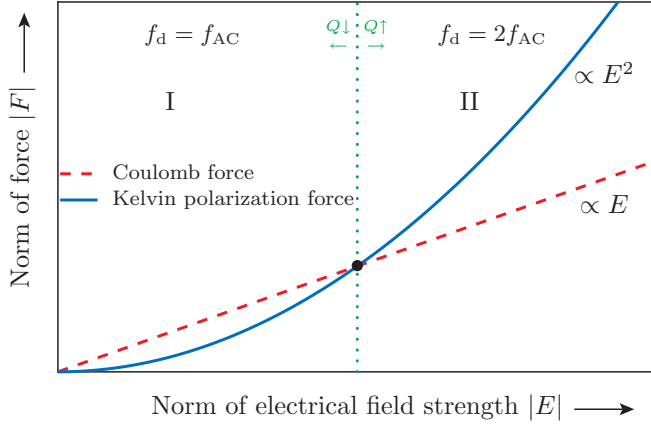


FIG. 2. Principle of acting forces depending on electric field strength and electric charge. Region I characterizes the behavior of charged and region II uncharged drops, adapted and reprinted with permission from [39].

the charges induced by the field itself, similar to the second term on the right side of Eq. (3) [38]. Additional charges on the drop result in an additional stress σ_Q due to the electric field

$$\sigma_Q = qE, \quad (4)$$

where q is the electric charge per area of the drop.

Comparing Eqs. (3) and (4) indicates that the oscillation and deformation of the drop depends on the electric charge and on the applied electric field strength. Consequently, one of the forces can be predominant depending on the boundary conditions. In the case of an alternating electric field, the dominating force determines the oscillation frequency f_d of the drop. Assuming a sinusoidal electric field, uncharged drops should oscillate with twice the frequency f_{AC} of the applied voltage, as indicated by Eq. (3), due to $f_d \propto \sigma \propto E^2 \propto 1 - \cos(2\omega)$. Even if the drop is assumed as perfect conductor, the net force produced by the nonhomogeneous electric field leads to the same outcome. In contrast, charged drops should oscillate with the same frequency f_{AC} as the applied voltage, due to $f_d \propto \sigma \propto E \propto \sin(\omega)$. Figure 2 shows the expected correlation between the forces on the drop, the electric field strength, and the electric charge. The behavior of the drops can be divided into two different regions to distinguish between the different oscillation frequencies of the droplet and to characterize the behavior. Region I contains drops oscillating with the same frequency as the applied voltage and region II contains the drops with the doubled frequency. Both forces, Coulomb and Kelvin polarization forces, act on the drop simultaneously, and the behavior of the drop is defined by the charge and the applied electric field strength. Consequently, both the electric charge and the field strength have to be taken into account to accurately describe the behavior of drops within electric fields.

The amount of charge carried by the drop depends on the experimental conditions and drop handling. Thus, the behavior of charged drops under the impact of electric fields has to be investigated under well-defined conditions, including the charge on the drop, the surface charge of supporting substrate,

TABLE I. Overview of the tested parameters including their quantities. The frequency of the electric field depends on the drop volume and was chosen according to Eq. (2) for each volume. In addition, the applied electric charge also varies with the drop volume. A detailed summary of the electric charge depending on the drop volume and the frequency of the electric field can be found in the Supplemental Material [35].

Variable	Quantity
Volume V in μl	20, 40, 60, 80
Kinematic viscosity ν in m^2/s	1.004×10^{-6} , 1.88×10^{-6}
Electric field strength \hat{E} in kV/cm	2.58, 4.42, 7.37
Frequency of electric field f_{AC} in Hz	27.77, ..., 83.3
Electric charge Q in nC	0, ..., 3.36

as well as the drop handling, to ensure realistic reproduction of experiments. Furthermore, the interaction between the drop charge as well as the electric field strength and the drop is important to improve the understanding of the behavior and to be able to manipulate the behavior of drops. This might also explain unclear phenomena from previous experiments in literature and consequently increase the understanding of water drops in electric fields.

In this experimental work, the behavior of charged drops under well-defined conditions is investigated to determine the impact of the charge depending on the drop volume as well as the electric field strength. Charged and uncharged drops with a volume between 20 and 80 μl are investigated under the impact of an alternating electric field tangentially aligned to the substrate with a high-speed camera.

To determine the impact of charges on the behavior of the drop, the first three resonance frequencies of the sessile drops are investigated in detail. Both the electric charge as well as the field strength are varied over a wide range from $Q = 0$ nC to $Q \approx 3.5$ nC and $\hat{E} = 0$ kV/cm^{-1} to $\hat{E} \approx 7.4$ kV/cm^{-1} , respectively. A summary of all test parameters can be found in Table I and in the Supplemental Material [35]. For the given setup, the charge is limited by the fact that a drop of specific size can only contain a limited charge, which is given by the Rayleigh limit [1]

$$Q_{\max} = \sqrt{48\pi\epsilon_0\gamma V}. \quad (5)$$

Charges in the order of the Rayleigh limit result in deformation or disintegration of the drop on the substrate and, therefore, cannot be investigated. In addition, the electric field strength is also limited because high electric fields ($\hat{E} > 7.4$ kV/cm^{-1}) might lead to drop deformation and contact line motion of the drop. Consequently, the large oscillations of the drop leads to large contact angle variations and might cause drop spreading if the advancing contact angle is reached. The spreading of the drop depends also on the local surface properties and is often given by a stick-slip motion due to the periodic oscillation. Lower electric field strength, which does not lead to the motion of the drop, only influences the amplitude of the oscillation. The higher the electric field strength, the higher is the amplitude of the oscillation. This work only takes drops with pinned three-phase contact line into account, due to the fact that only the oscillation of

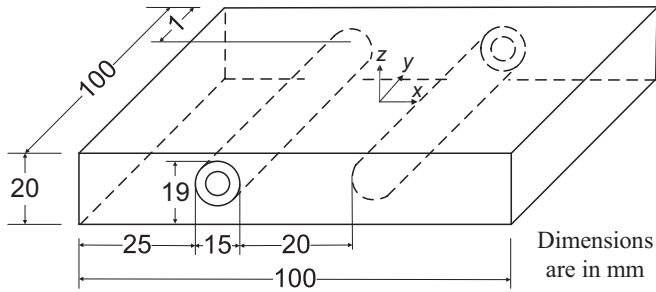


FIG. 3. Schematic of the specimen, similar to [40].

the drop should be analyzed. Depending on the motion and deformation of the drop, the impact of the charges and the field strength is analyzed. The aim is to quantify the amount of charge and the corresponding field strength to change and control the behavior of drops inside strong electric fields, resulting in an enhanced understanding of the behavior of drops inside of electric fields.

II. EXPERIMENTAL SETUP

Sessile drops are investigated inside an alternating electric field tangentially aligned to the surface of the substrate. A generic, cuboidic insulator is used as a specimen/substrate, which consists of silicone rubber (Wacker Powersil 600) with a size of $10\text{ cm} \times 10\text{ cm} \times 2\text{ cm}$ ($l \times w \times h$), which is shown in Fig. 3. The silicone rubber is widely used for high-voltage insulators and has a high breakdown strength (23 kV/mm), high tracking resistance (1A 3.5 according to IEC 60587), as well as hydrophobic surface properties. A casting mould is used to produce the specimen, resulting in a smooth silicone rubber surface as can be found on high-voltage composite insulators. Two rod electrodes are embedded into the silicone rubber with a diameter of $d_{\text{elec}} = 15\text{ mm}$ and a distance of $h = 20\text{ mm}$ to generate a tangentially aligned electric field on the substrate's surface. To increase the creeping distance, the electrodes are embedded from opposite sides as shown in Fig. 3. A voltage up to $U = 20\text{ kV}$ is applied between both electrodes to achieve a maximum field strength of about $\hat{E} = 7.4\text{ kV cm}^{-1}$. The high voltage is generated using a function generator, an amplifier, and a single-phase high-voltage transformer. The function generator is used to create a sinusoidal signal with a frequency between 20 and 100 Hz, corresponding to the specific resonance frequencies of the drops. Prior to the drop deposition, the surface of the specimen is cleaned using antistatic wipes soaked in isopropanol to ensure a dust-free substrate and to minimize surface charges [27] as well as to ensure a low surface conductivity. Thus, the charge transfer from the substrate to the drop is reduced and almost negligible due to the small amount of charge as well as the large timescale for the charge transfer [27]. An example for the surface charge distribution on the substrate is shown in Appendix C. The cleanness of the surface as well as the surface charge distribution of the substrate influence the wetting properties of the drop. Hence, the shape of the drop is checked prior to the experiment and in case of a deformation or asymmetric wetting, the drop is replaced. Furthermore, large variations due to a contaminated surface are recognized during the analysis of the video because of the high image

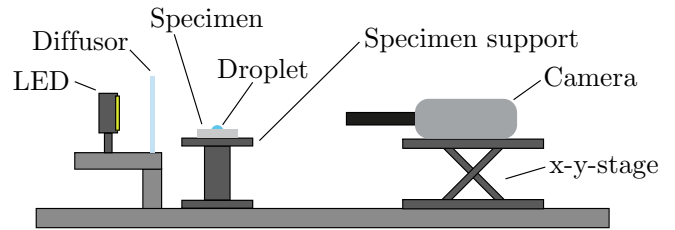


FIG. 4. Schematic of the experimental setup.

resolution. In doubt the experiment is repeated and compared to the previous run to ensure a high repeatability.

The movement of the drop is captured by a high-speed camera (Phantom V12) with a frame rate of up to 4000 fps using shadowgraphy as shown in Fig. 4. The video data are used to analyze the two-dimensional motion of the drop inside the x - z plane (see Fig. 3). In addition to the video data, the applied alternating voltage as well as ambient conditions are recorded using a data acquisition system by National InstrumentsTM. The analysis of the video data is performed by an in-house code developed in MATLAB, which analyzes the drop area, center of mass, deformation in height and width, curvature of the drop surface, as well as the contact angle, depending on temporally resolving edge detection algorithms and morphological operations. The corresponding frequencies are determined by a fast Fourier transformation (FFT) of the time dependent signals. An example of the detected shape as well as the corresponding signal for the contact angle is shown in Appendix B.

The analysis of the different signals and the automated detection of the oscillation frequency is sometimes not completely clear, especially in case of asymmetric drop motion. Consequently, a well-defined and characteristic parameter has to be used for the analysis. For sessile drops, the center of mass is always coupled with the motion of the drop [41], and therefore serves this purpose. Nevertheless, the two-dimensional motion of the drop is not necessarily coupled, so that different frequencies may occur for different directions of motion. Hence, the principal direction of motion is used as a reference to determine the corresponding frequency. It is important to note that especially for the first asymmetric motion of the drop (first resonance frequency), a careful analysis of the motion is necessary. In contrast to the resonance frequencies of higher orders, the principal motion is not vertical but horizontal. In case of mixed motion and modes, the principal motion is determined by the analytical mode given by Eq. (2) as well as the characteristic motion shown in Fig. 1. Consequently, for mode 1 the horizontal motion and for higher modes the vertical motion is defined as principal motion.

Generation of charged and uncharged drops

The drops consisting of high-purity water (Millipore Milli-Q Type I with an electric conductivity of $\gamma_{\text{el}} = 5.5 \times 10^{-6}\text{ S/m}$ at 25°C) are generated by using an automated syringe (Hamilton 1710 RN), which ensures a constant flow rate and accurate control of the drop volume with $\Delta V \approx 5\%$ of the desired volume. To generate uncharged drops, the metallic needle of the syringe is grounded. Charged drops

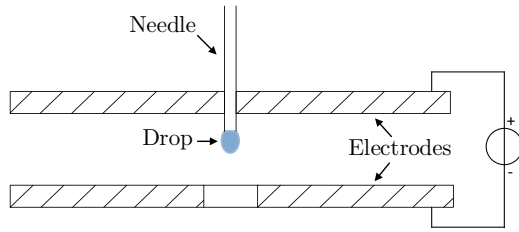


FIG. 5. Schematic of the drop charger [39].

are generated by using a drop charger similar to [42]. A schematic of the experimental setup is shown in Fig. 5. Two plate electrodes with a distance of 5 mm are used to generate a constant electric field using a high-voltage source (Heinzinger PNChp 20000). The metallic needle of the syringe punctures the high-voltage electrode. Water is forced to flow through the needle using the automated syringe, and due to the electric field the drop is charged by charge separation. As soon as the sum of the electric force and gravity is larger than the surface tension, the drop detaches from the needle and leaves the drop charger through a hole in the grounded electrode. The resultant charge depends on the applied voltage, the drop volume, as well as the used flow rate. To accurately determine the relation between the applied voltage and the drop volume, the drop charger is calibrated using a Faraday cup [28,42] and an electrometer (Keithley 6514) to ensure an accurate determination of the actual charge on the drop. The calibration result is shown in Appendix A (see Fig. 16). Consequently, drops with a well-known charge can be produced with an accuracy of $\Delta Q \leq 5.5$ pC. The drop charger is placed above the specimen without touching the substrate to prevent the generation of surface charges. Thus, a detached drop falls onto the substrate exactly at its center to ensure a repeatable drop position and that the drop is influenced by a well-defined electric field.

III. RESULTS

Aside from the electric field strength, the volume, the electric charge, and the drop motion as well as the resonance mode influence the behavior of the drop inside an electric field tangentially aligned to the substrate. To determine the influence

of the drop motion, the first three resonance modes of sessile drops are investigated in detail for uncharged and charged drops. Due to the fact that an ideal uncharged drop cannot be produced, both the dielectric and electrostrictive as well as the force due to electric charges always appear simultaneously. Even uncharged drops always contain residual charges, which are in this work quantified by $Q < 5.5$ pC. The resonance frequency of the drop depends on the drop volume as well as the properties of the liquid. Depending on the oscillation mode, the motion of the drop can be horizontal (mode 1) as well as vertical (modes 2 and 3). Hence, several frequencies might be superimposed on the drop motion, depending on the analyzing criteria, as will be seen by the different peaks in Appendix B [Fig. 18(b)].

The behavior of the drop can be characterized by two dimensionless numbers. The motion of the drop is described by the frequency ratio

$$f_d/f_{AC}, \quad (6)$$

where f_d is the frequency of the drop in the principal direction of motion for the corresponding mode. Note that the principal direction of motion is horizontal for mode 1 and vertical for all other modes. f_{AC} is the frequency of the applied sinusoidal voltage. Therefore, the ratio characterizes whether the drop oscillates with the same or a multiple of the frequency of the applied voltage. The motion of the drop is influenced by the charge of the drop, the electric field strength, as well as the volume of the drop. Therefore, a dimensionless number ξ is introduced

$$\xi = \frac{Q}{\epsilon_0 \hat{E} d^2}, \quad (7)$$

where Q is the charge of the drop. The ratio characterizes the forces due electric charges as well as the dielectric and electrostrictive forces. Using the dimensionless ratios, the drop behavior can be analyzed in detail, and the interaction of the different influencing factors can be determined. It is noteworthy that for a high electric field strength E as well as high drop volumes, corresponding to large diameters d , the ratio ξ is very small. Similarly, a large amount of charge increases the ratio. Hence, the ratio ξ increases for a fixed electric field strength and volume for increasing charge of the drop.

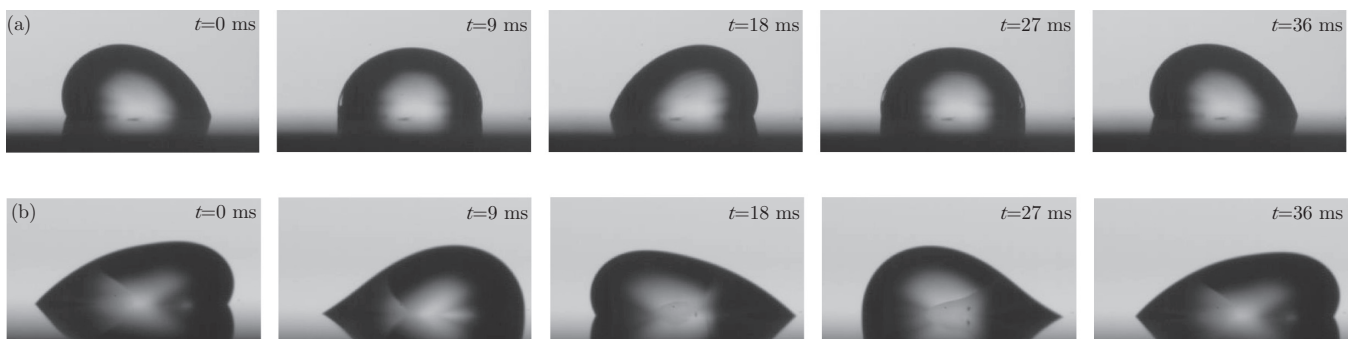


FIG. 6. Comparison of one cycle of an uncharged and a charged drop in resonance mode 1. (a) One cycle of an uncharged drop with a volume of $V = 20 \mu\text{l}$ and a voltage frequency of 27 Hz at an electric field strength of $\hat{E} = 3.81$ kV/cm and (b) one cycle of a charged drop ($Q = 0.646$ nC) with a volume of $V = 20 \mu\text{l}$ and a voltage frequency of 27 Hz at an electric field strength of $\hat{E} = 4.42$ kV/cm. The videos can be found in the Supplemental Material [35].

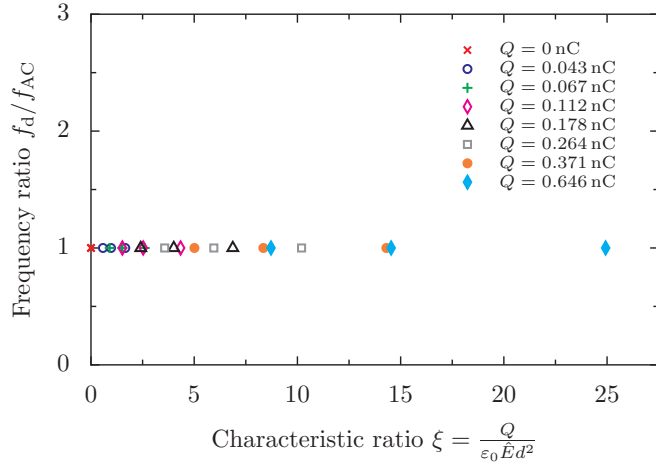


FIG. 7. Dimensionless frequency ratio depending on the characteristic ratio ξ for a drop oscillating in mode 1 with $V = 20 \mu\text{l}$.

A. Mode 1

In contrast to higher modes, the first resonance mode of the sessile drop, often called rocking [43], ratchetlike [44], or bending motion [45], leads to a nonaxisymmetric motion (see Fig. 1). The resonance frequency is defined by Eq. (2) using $n = 2$. In this case, the drop always has the same frequency as the applied voltage independent of the charge of the drop. Figure 6 shows an example of a cycle of an uncharged and a charged drop with a volume $V = 20 \mu\text{l}$ at a frequency of 27 Hz. The motion of the drop is independent from the actual net charge on the drop and the drop volume, so that even high charges and a small electric field strength do not change the behavior of the drop.

Figure 7 shows exemplarily the dimensionless frequency ratio f_d/f_{AC} depending on the dimensionless ratio ξ and the drop charge for a drop with the volume of $V = 20 \mu\text{l}$. The frequency of the drop in the horizontal direction is always the same as the applied frequency of the applied voltage, even for uncharged drops. Hence, the drop always behaves as a charged drop in mode 1 independent of its charge. Nevertheless, in the vertical movement of the drop, the doubled frequency of the applied voltage can always be recognized. The behavior of the drop in mode 1 is independent of the drop volume, the electric charge, as well as the electric field strength for the tested parameters and always has the same frequency as the applied voltage. A change of the frequency was not recognized over the wide range of the tested parameters. Therefore, no onset charge could be determined as shown in Fig. 8, which shows the minimum dimensionless onset charge Q^*/Q_{\max} depending on the dimensionless drop volume represented by the Bond number Bo . For mode 1, no change in behavior was recognized so that all drops oscillate with the same frequency as the applied voltage, which is characterized by region I. Depending on the position of the drop in the electric field and the precision of the drop volume as well as the charge of the drop, a superposition of modes 1 and 2 may be observed. In this case, both frequencies, the single as well as the doubled frequency, can be observed depending on the direction of motion. Hence, the drop motion is very sensitive to changes of the influencing parameters. It is worth noting

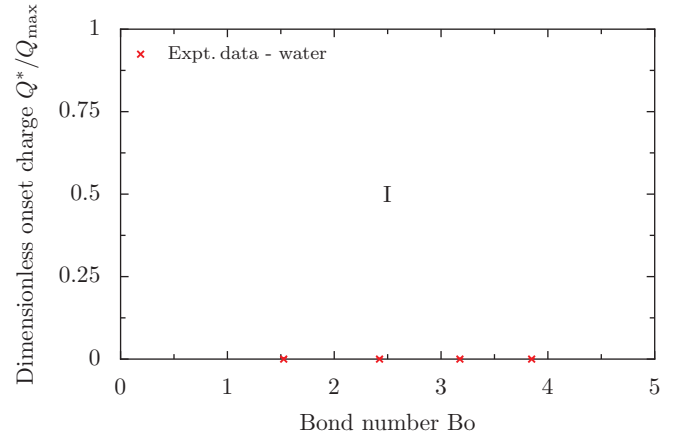


FIG. 8. Minimum dimensionless onset charge depending on the dimensionless drop volume represented by the Bond number.

that the motion of the drop in mode 1 is completely different from the higher modes due to the fact that mode 1 is the only motion, which is nonaxisymmetric.

B. Mode 2

The principal motion of mode 2 ($n = 3$) is given by a vertical motion. The motion is influenced by the drop charge as well as the applied electric field strength. Figure 9 shows the motion of an uncharged and a charged drop oscillating in mode 2. A drop with a volume of $V = 80 \mu\text{l}$ without charge oscillates with double the frequency of the applied voltage ($f = 26 \text{ Hz}$) for a high electric field strength. Increasing the charge leads to a decrease of the oscillation frequency, especially for small electric field strengths, as shown in Fig. 9. Furthermore, an increase of the electric field strength for a constant volume but slightly higher charges again leads to a change of the frequency. It is important to note that increasing the charge requires an even higher electric field strength to change the behavior. The reason for this behavior is the increase of the dielectric and electrostrictive forces, which are higher than the Coulomb force in this case. In addition, the drop shape is affected by the electric field and might be more widely spread on the substrate as shown in Fig. 9(c). Even though the footprint of the drop is larger, the contact line is still pinned during the oscillation. However, an even higher field strength would cause a further drop spreading and motion. Consequently, the behavior of the drop depends on the volume, the electric charge, as well as the electric field strength.

Figure 10 shows the frequency ratio depending on the dimensionless ratio of the force due to electric charges and the dielectric and electrostrictive forces depending on the drop charge, exemplarily for a drop with a volume of $V = 60 \mu\text{l}$. For a high electric field strength and small amount of charge, which corresponds to small values of ξ , the drop oscillates with double the frequency of the applied voltage, as expected. Increasing the charge of the drop results in an increasing ξ , which can lead to a change of the behavior. A change of the behavior for a drop with a volume of $V = 60 \mu\text{l}$ is given for $\xi^* > 18.47$. For values larger than ξ^* , the drop has the

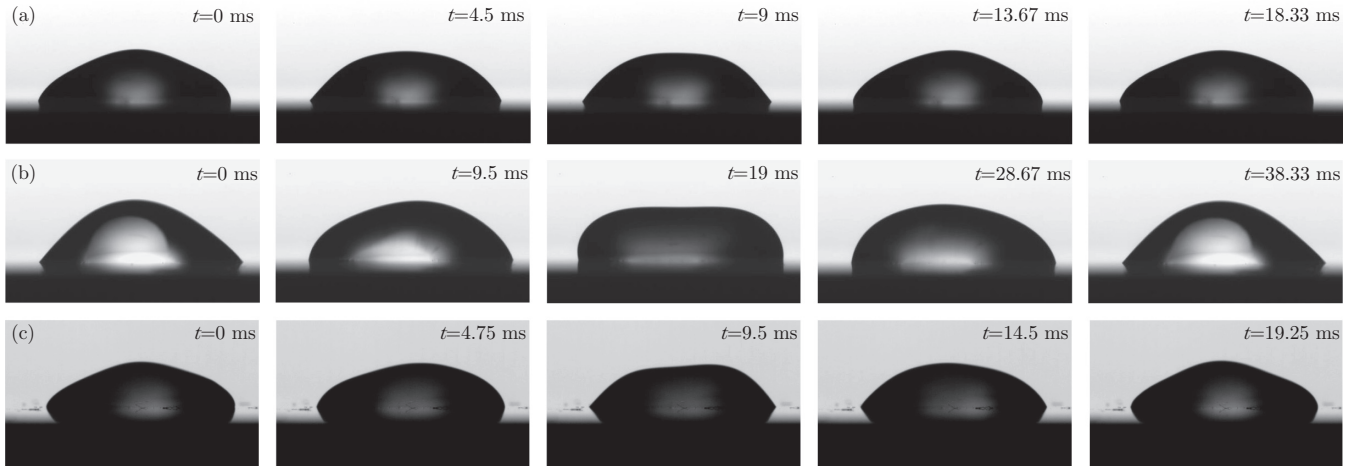


FIG. 9. Comparison of one cycle for an uncharged and a charged drop in resonance mode 2. (a) One cycle of an uncharged drop with a volume of $V = 80 \mu\text{l}$ and a voltage frequency of 26 Hz at an electric field strength of $\hat{E} = 7.37 \text{ kV/cm}$, (b) one cycle of a charged drop ($Q = 2.76 \text{ nC}$) with a volume of $V = 80 \mu\text{l}$ and a voltage frequency of 26 Hz at an electric field strength of $\hat{E} = 2.58 \text{ kV/cm}$, and (c) one cycle of a charged drop ($Q = 3.36 \text{ nC}$) with a volume of $V = 80 \mu\text{l}$ and a voltage frequency of 26 Hz at an electric field strength of $\hat{E} = 7.37 \text{ kV/cm}$. The videos can be found in the Supplemental Material [35].

same frequency as the applied voltage. The same behavior was observed for the other tested volumes. Consequently, a minimum amount of charge Q^* can be defined, which can lead to a frequency change of the drop as seen in Fig. 10. It is noteworthy that the change of the behavior depends on both the minimum charge Q^* and the corresponding electric field strength. If the electric charge of the drop is smaller than the required charge, the drop behaves as an uncharged drop and oscillates with twice the frequency of the applied voltage. Larger charges reduce the oscillation frequency to the same as the applied voltage. Note that increasing the electric field strength will always lead to a change of the behavior due to the fact that the dielectric and electrostrictive forces will be dominant. Consequently, the interaction between charges and the electric field has to be considered for the oscillation of drops inside of electric fields. The given value of ξ^* for

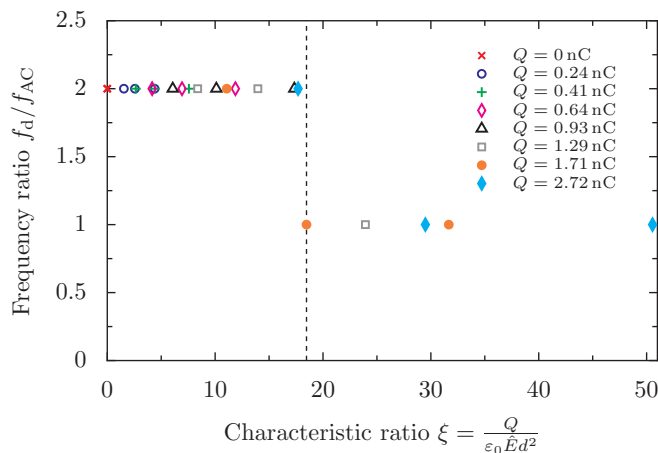


FIG. 10. Dimensionless frequency ratio depending on the characteristic ratio ξ for a drop oscillating in mode 2 with $V = 60 \mu\text{l}$. Dashed line shows the characteristic ratio ξ^* for the change of the behavior, reprinted with permission from [39].

the change of the behavior depends on the drop volume and might not be a fixed value as shown in Fig. 10. In most cases, an intermediate regime appears, where single and double frequency motion can occur for the same value of ξ .

The amount of charge of a drop that can be applied is correlated with the drop volume. Increasing the drop volume also increases the amount of charge that can be applied to the drop, as indicated by Eq. (5). Hence, it is expected that the onset charge for the change of the drop behavior increases with increasing volume. Figure 11 shows the minimum onset charge Q^* for the drop behavior change for different drop volumes and fluids. Region I in Fig. 11 contains charged

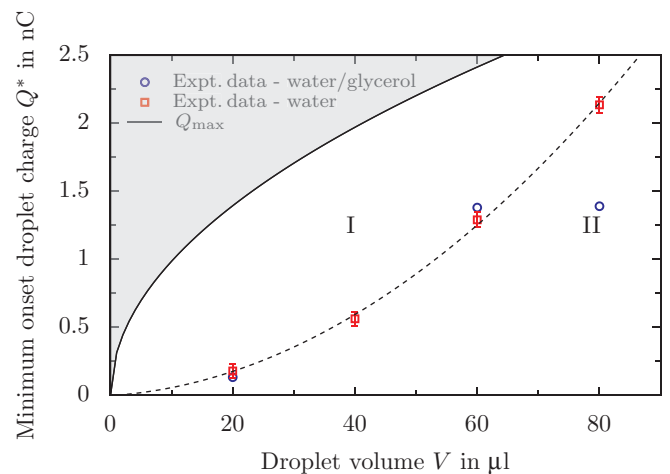


FIG. 11. Minimum onset charge Q^* for frequency change depending on the drop volume V compared with Q_{max} as defined by Eq. (5) for mode 2 and different viscosities. Data for pure water are taken from [39]. Regime I includes drops with same frequency and regime II drops with double the frequency of the applied voltage. Dashed line visualizes the two regimes. The solid line limits region I due to the Rayleigh limit, therefore, the gray area includes nonphysical values.

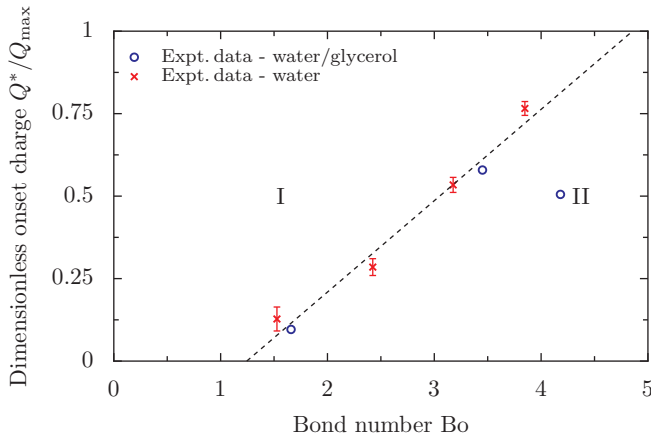


FIG. 12. Dimensionless onset charge Q^*/Q_{\max} depending on the Bond number Bo for drops oscillating mode 2. Regime I includes drops with same frequency and regime II doubled frequency of the applied voltage. Dashed line visualizes the two regimes.

drops with the same frequency as the applied voltage, which is limited by the Rayleigh limit and is shown as a solid line. The gray region includes all drop charges, which are higher than the Rayleigh limit and cannot be reached in practice due to disintegration of the drop. Region II characterizes the behavior of uncharged drops. It is worth noting that even charged drops can behave as uncharged drops as indicated by region II. The amount of charge for the frequency change depends on the drop volume, so that the charge increases with increasing drop volume. Figure 11 shows the transition between both regions as a dashed line, which is given by a quadratic fit of the experimental data of pure water and indicates an increasing charge-to-mass ratio Q/m . Hence, the ratio is not constant for the different drop volumes.

In addition to water, a mixture of glycerol and water was investigated to determine the influence of the viscosity.

Glycerol is used due to its properties similar to water, i.e., surface tension ($\gamma_{\text{gly}} = 63.4 \times 10^{-3} \text{ N/m}$) and density ($\rho_{\text{gly}} = 1260.8 \text{ kg/m}^3$). A mixture with a mass fraction of 25 ml glycerol and 100 ml water was used, resulting in a viscosity of the mixture $\nu_{\text{mix}} = 1.878 \times 10^{-6} \text{ m}^2/\text{s}$ at 20°C , which is almost twice the viscosity of pure water, and a permittivity of $\epsilon \approx 73$ taking into account the mass fraction as well as the permittivity of pure glycerol ($\epsilon \approx 42$) and water ($\epsilon \approx 82$). Nevertheless, the minimum onset charge is not influenced by the viscosity or changed permittivity, as shown by the blue circles. The lowered permittivity leads to a smaller force on the drop compared to pure water but does not influence the general behavior. In addition, the influence of the viscosity can be neglected for small drop volumes, and the behavior is only determined by surface tension and gravity. For increasing drop volumes $V > 80 \mu\text{l}$ the viscosity seems to have an effect.

Figure 12 presents the data shown from Fig. 11 in dimensionless form using Q_{\max} as a scale for Q^* . The ratio Q^*/Q_{\max} is plotted as a function of the Bond number Bo , defined in Eq. (1). Region I indicates the drop movement with the same frequency and region II with the doubled frequency of the applied voltage. The onset charge increases with increasing volume. Region I is limited by the maximum charge (Rayleigh limit, $Q^*/Q_{\max} = 1$), but also depends on the electric field strength. An increase of the electric field strength leads to a smaller region I for a constant drop volume. Especially for large drop volumes, which correspond to high Bond numbers, region I can be very narrow or not present at all (e.g., approximately $Bo > 4.9$). Hence, the influence of the charge is much bigger for smaller drops and high electric field strengths. The dependence of the dimensionless onset charge and the Bond number is almost linear, only for high Bond numbers and increased viscosity the dimensionless onset charge seems to decrease again. The error bars shown in Fig. 12 show the measurement uncertainty given by the uncertainty of the charge measurement, the drop volume, as well as the measurement of the applied voltage. Consequently,

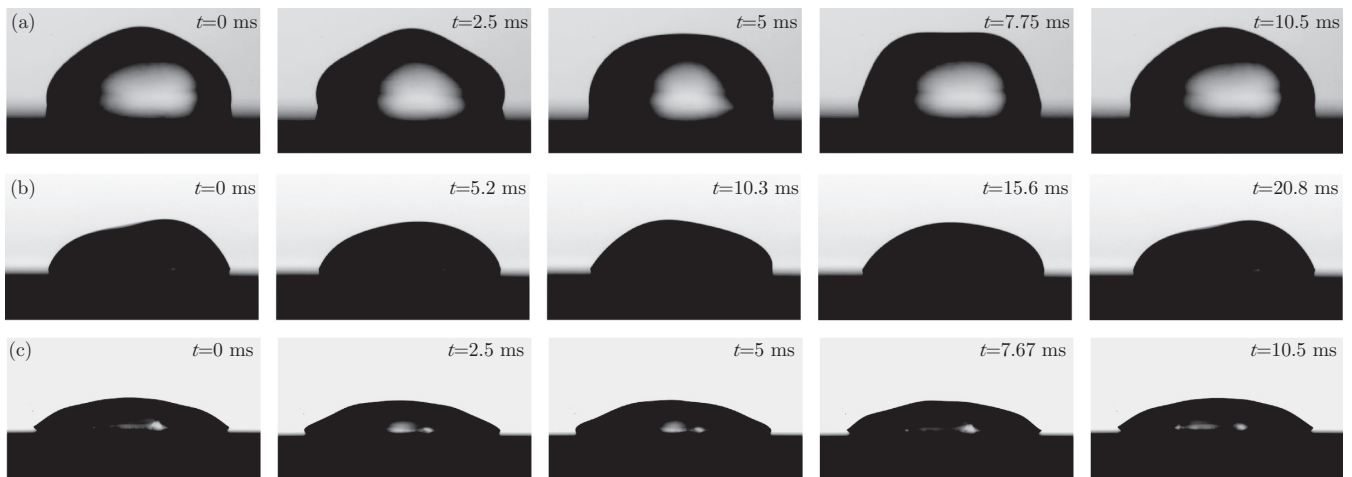


FIG. 13. Comparison of one cycle for an uncharged and a charged drop in resonance mode 3. (a) One cycle of an uncharged drop with a volume of $V = 60 \mu\text{l}$ and a voltage frequency of 48 Hz at an electric field strength of $\hat{E} = 7.37 \text{ kV/cm}$, (b) one cycle of a charged drop ($Q = 3.69 \text{ nC}$) with a volume of $V = 60 \mu\text{l}$ and a voltage frequency of 48 Hz at an electric field strength of $\hat{E} = 2.58 \text{ kV/cm}$, and (c) one cycle of a charged drop ($Q = 2.72 \text{ nC}$) with a volume of $V = 60 \mu\text{l}$ and a voltage frequency of 48 Hz at an electric field strength of $\hat{E} = 7.37 \text{ kV/cm}$. The videos can be found in the Supplemental Material [35].

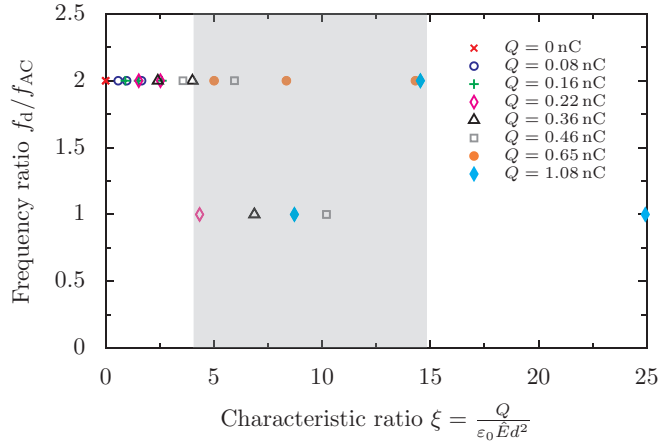


FIG. 14. Dimensionless frequency depending on the characteristic ratio ξ for a drop oscillating in mode 3 with $V = 20 \mu\text{l}$. Gray area shows the transition regime.

the behavior of drops under the impact of electric fields can be manipulated by changing the drop volume, the charge, and the electric field strength.

C. Mode 3

Figure 13 shows the motion of a drop with a volume of $V = 60 \mu\text{l}$ in mode 3 with and without charge. An uncharged drop oscillates with the doubled frequency of the applied voltage (48 Hz). In case of low electric field strengths, increasing the charge reduces the oscillation frequency to the same frequency as the applied voltage, similar to mode 2, as shown in Fig. 13(b). Increasing the electric field strength leads to another frequency change due to the high dielectric and electrostrictive forces. Similarly, the drop shape is influenced by the electric field, and the footprint might also be increased. Figure 13(c) shows an example of the changed behavior and increased footprint. It is also shown that the oscillation of the drop is reduced with a high electric field strength and high electric charge due to the high forces which are stretching the drop. The surface tension prohibits large oscillations of the surface. Even if the charge is slightly reduced [Fig. 13(c) compared to Fig. 13(b)], the change in behavior can also be observed for higher charges but with an eventually increased electric field strength. Figure 14 shows the dimensionless frequency ratio for a drop with a volume of $V = 20 \mu\text{l}$ in resonance mode 3. As already mentioned, the change in behavior does not occur for a fixed characteristic ratio. The gray area shows the transition regime, which is rather large. It is important to mention that for a drop with a volume of $V = 60 \mu\text{l}$ the transition occurs for the same value as for mode 2. The large transition regime might be caused by a charge transfer between the insulator and the drop and, therefore to changed boundary conditions. For a large transition regime, the lowest charge for the change in behavior is used as characteristic value. Hence, the change of behavior is given for a minimum onset charge of $Q^* = 0.22 \text{ nC}$ and a value of $\xi^* = 4.34$.

As already shown for mode 2, the frequency of the drop does not only depend on the electric charge, but also on

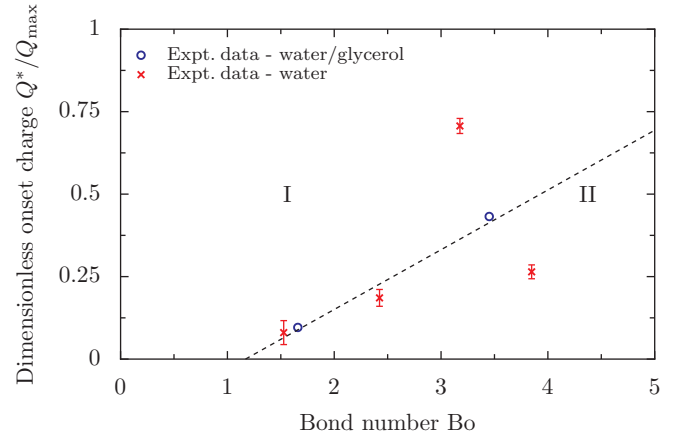


FIG. 15. Dimensionless onset charge Q^*/Q_{max} depending on the Bond number Bo for drops oscillating in mode 3. Regime I includes drops with same frequency and regime II with double the frequency of the applied voltage. Dashed line visualizes the two regimes.

the electric field strength. Figure 15 shows the dimensionless onset charge in dependence on the Bond number. The general behavior is the same as for mode 2. An increasing drop volume leads to an increasing characteristic ratio to change the oscillation behavior. Regime I is also limited by a maximum value of $Q^*/Q_{\text{max}} = 1$, which is defined by the maximum charge given by the Rayleigh limit and the electric field strength. An increase of the electric field strength leads to a diminishment of region I. Simultaneously, the slope of the transition line between regions I and II is lower compared to mode 2, which enables larger drops to oscillate with the same frequency as that of the applied voltage, as shown for mode 2. Hence, the electric field strength has a strong influence on the behavior of larger drops. Comparing the values for Q^*/Q_{max} between modes 2 and 3 shows that they are of the same order. For large Bond numbers $Bo > 3$ the scatter of the data is larger, as already seen in Fig. 15. Hence, the presented theory is only valid for small drop volumes. For small volumes, regime II is larger for mode 3 compared to mode 2. Therefore, it is more likely for small drops to oscillate with the same frequency as that of the applied voltage.

IV. CONCLUSIONS

The behavior of drops under the impact of an alternating electric field depends on several influencing factors like oscillation mode, volume, electric charge, as well as the electric field strength. In the first resonance mode sessile drops always oscillate with the same frequency as that of the applied voltage independent of the electric charge and electric field strength. In contrast, higher modes are highly influenced by the electric charge of the drops as well as the electric field strength. The behavior of drops oscillating in modes 2 and 3 is rather similar. An increasing drop volume results in an increased charge to force the drop to oscillate with the single frequency. Furthermore, a high electric field strength always leads to the doubled frequency of the drop compared to the applied voltage, which is in good agreement with the presented theory. Hence, the frequency of the drop can be influenced by the boundary

conditions. Especially, small drops are highly influenced by electric charges. The influence of the viscosity on the onset charge is almost negligible and only influences the behavior of the larger drops.

Based on the experiments, a regime map for the different modes and the onset charge for the change in behavior was determined. The change of behavior depends on the electric charge as well as on the electric field strength and is characterized by a transition regime. For special cases, the transition regime is given by a specific value of the characteristic ratio, which quantifies the force due to charge and the dielectric and electrostrictive forces. The presented model is in good agreement for drops with small volumes. For larger drop volumes, additional influencing factors affect the drop behavior. The necessary charge for the change in behavior is rather low compared to the maximum possible charge (Rayleigh limit) and, therefore, is very common in many applications or in nature like charged raindrops [46]. Consequently, the behavior of charged and uncharged drops is important for many applications, especially for the aging process of high-voltage insulators. The oscillation frequency of the drops might also influence the occurrence of partial discharges at the three-phase contact line. Hence, the insulating substrate might become deteriorated, which is a crucial problem, e.g., for high-voltage composite insulators. This study improves the understanding of the drop behavior under the impact of electric fields, especially under realistic conditions.

ACKNOWLEDGMENTS

The authors would like to thank the Deutsche Forschungsgemeinschaft (DFG) for financial support of the project within the Collaborative Research Centre SFB-TRR 75, Project No. 84292822. Furthermore, the authors like to thank F. Zajonz.

APPENDIX A: CALIBRATION OF THE FARADAY CUP

The charged drop is generated by the droplet charger and is placed on the insulator. The charge of the drop cannot be measured during the experiment. To ensure an accurate charge measurement, the droplet charger is calibrated using a Faraday cup as shown in [39]. The output of the Faraday cup is calibrated as well to ensure a high accuracy. Therefore, a charge calibrator (Kistler 5357 B) is used to apply charges between $Q = 1 \times 10^{-11}$ C and $Q = 7.5 \times 10^{-7}$ C directly to the Faraday cup. The charge is measured by an electrometer (Keithley 6514). The correlation between applied and measured charge is shown in Fig. 16.

The solid line shows the excellent agreement between applied and measured charges. The measurement data are given by the red crosses. Each individual measurement was performed at least three times. The error bars include the measurement uncertainty of the complete measurement chain. It is important to consider that the axes are logarithmic so that the errors in the small range ($Q \approx 10^{-11}$ C) appear larger compared to the higher range ($Q \approx 10^{-7}$ C) even though they are in the same order of magnitude. In addition, the impact of the polarity on the charge measurement was investigated, but no significant influence could be recognized. The measurement data have a high accuracy with a maximum

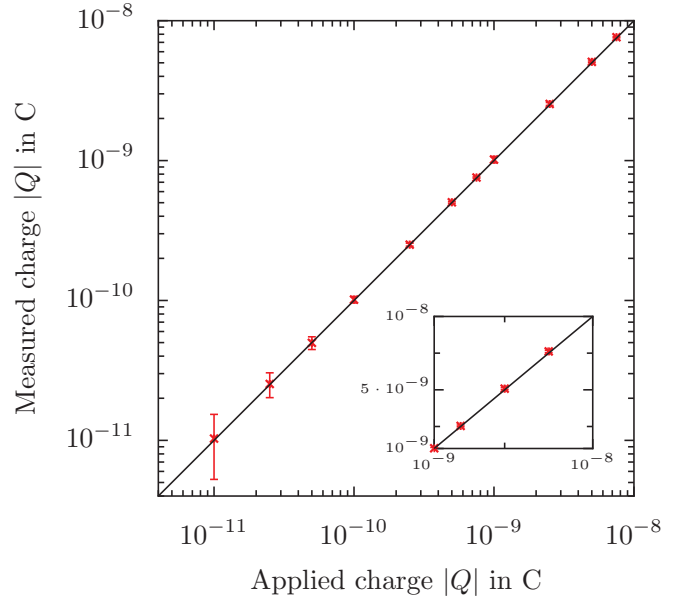


FIG. 16. Calibration of the Faraday cup. Comparison of applied and measured charges including the uncertainty of the measurements. The inset shows the range from $Q = 1 \times 10^{-9}$ C to $Q = 10 \times 10^{-9}$ C in detail.

error of $\Delta Q = 8.12 \times 10^{-9}$ C for the full range and $\Delta Q = 5.5 \times 10^{-9}$ C for the range used in this work.

APPENDIX B: ANALYSIS OF THE VIDEO DATA

The analysis of the video data is performed by an in-house MATLAB code. An exemplary result of the analysis is shown in Figs. 17 and 18.

Figure 17 shows a deformed drop, which is oscillating in the first resonance mode as well as the detected shape of the drop as indicated by the red boundary. Furthermore, the contact angle is determined for each image. Figure 18(a) shows the corresponding contact angle depending on time. In addition, several other parameters like the projected area, the center of the drop, or the deformation are determined by using the shape and boundary of the drop. These signals are analyzed using a FFT to determine the dominant frequencies of the signal. Especially for small deformations of the drops, the frequency analysis may not result in an explicit frequency due to the low signal-to-noise ratio. Figure 18(b) shows the determined frequencies of the contact angle signal, which consists of several frequencies. The dominant frequency is given by the same frequency as the applied field, but also the

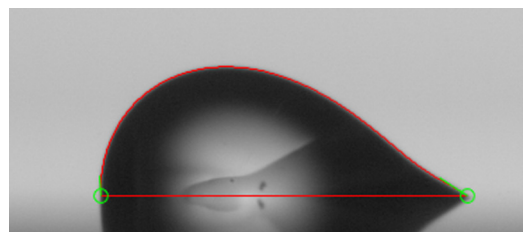


FIG. 17. Detected drop contour and contact angles.

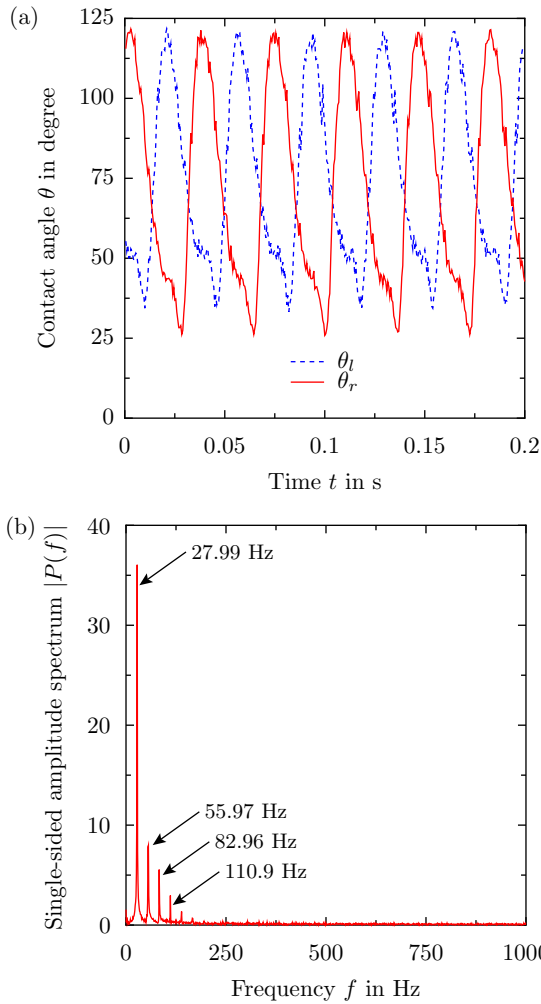


FIG. 18. Example of the analysis for a drop of a volume $V = 20 \mu\text{l}$ and a frequency of $f = 27 \text{ Hz}$. (a) Determined contact angles of the drop depending on time for several cycles. θ_r and θ_l are the right and left contact angle, respectively. (b) Single-sided amplitude spectrum of the determined contact angle θ_r . Signal consists of several signals of frequencies higher than $f = 27.7 \text{ Hz}$.

doubled frequency can be recognized, which proves that both forces are acting on the drop simultaneously. Hence, the frequency analysis of the additional data from, e.g., the projected area, center of mass in x and y directions, or a comparison of each frame and the detected number of pixels after subtracting the background are used to verify the frequency of the drop. In

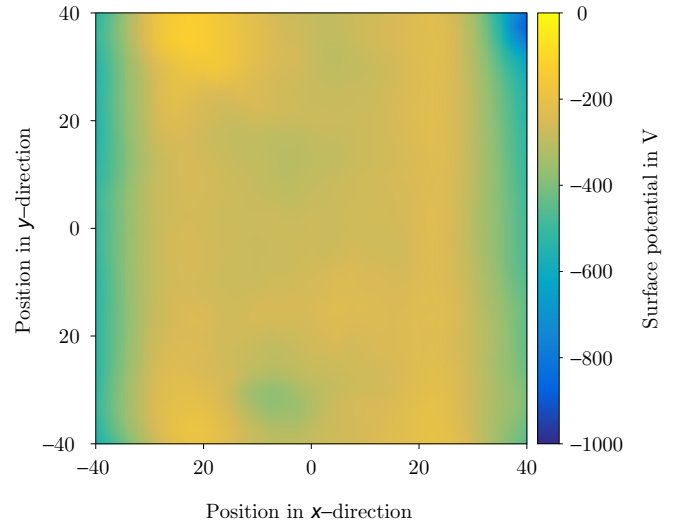


FIG. 19. Mean measured surface potential of cleaned surface of 10 measurements.

case of an ambiguous result from the automated analysis, the video data are analyzed by hand to determine the frequency. Consequently, the analysis of the oscillation of a drop has to be performed with caution and with respect to the general definition of an oscillation, which defines the period of the oscillation as the shortest time to repeat the exact and full motion, thus preventing a false detection of the video data. Especially, for mode 1 the analyzed data of, e.g., the contact angle can show the doubled frequency (repeating signal after a half period) even if the video data show a single frequency.

APPENDIX C: SURFACE CHARGE DISTRIBUTION

The silicone rubber used as substrate has a high affinity to accumulate charges on the surface, which might affect the electric field and the charge of the drop. To ensure repeatable and well-defined conditions, the surface of the substrate is cleaned with antistatic wipes soaked in isopropanol. Consequently, dust particles are removed from the substrate without residua. The isopropanol evaporates in a short time generating a clean and dry substrate. Different cleaning procedures including dry wipes, neutralization by free ions, cleaning with deionized water, and conductive brushes were tested. Only the chosen procedure showed a significant reduction and homogenization of the surface charges on the substrate. Figure 19 shows the mean surface potential distribution of a cleaned substrate for 10 measurements.

[1] L. Rayleigh, *Philos. Mag. Series 5* **14**, 184 (1882).
 [2] R. A. Millikan, *Phys. Rev.* **2**, 109 (1913).
 [3] G. Taylor, *Proc. R. Soc., A* **291**, 159 (1966).
 [4] S. Torza, R. G. Cox, and S. G. Mason, *Philos. Trans. R. Soc., A* **269**, 295 (1971).
 [5] F. Mugele and J.-C. Baret, *J. Phys.: Condens. Matter* **17**, R705 (2005).
 [6] L. Chen and E. Bonaccorso, *Adv. Colloid Interface Sci.* **210**, 2 (2014).

[7] M. W. Lee, S. S. Latthe, A. L. Yarin, and S. S. Yoon, *Langmuir* **29**, 7758 (2013).
 [8] A. M. Ganan-Calvo, J. M. Lopez-Herrera, N. Rebollo-Munoz, and J. M. Montanero, *Sci. Rep.* **6**, 32357 (2016).
 [9] J. Doshi and D. H. Reneker, *J. Electrostat.* **35**, 151 (1995).
 [10] M. Girault, H. Kim, H. Arakawa, K. Matsuura, M. Odaka, A. Hattori, H. Terazono, and K. Yasuda, *Sci. Rep.* **7**, 40072 (2017).
 [11] S. H. Tan, F. Maes, B. Semin, J. Vrignon, and J.-C. Baret, *Sci. Rep.* **4**, 4787 (2014).

- [12] H.-D. Xi, W. Guo, M. Leniart, Z. Z. Chong, and S. H. Tan, *Lab Chip* **16**, 2982 (2016).
- [13] I. Hayati, A. I. Bailey, and T. F. Tadros, *Nature (London)* **319**, 41 (1986).
- [14] M. R. Morad, A. Rajabi, M. Razavi, and S. R. P. Sereshkeh, *Sci. Rep.* **6**, 38509 (2016).
- [15] A. J. Phillips, D. J. Childs, and H. M. Schneider, *IEEE Trans. Power Deliv.* **14**, 1081 (1999).
- [16] J. P. Reynders, I. R. Jandrell, and S. M. Reynders, *IEEE Trns. Dielectr. Electr. Insul.* **6**, 620 (1999).
- [17] T. Schütte and S. Hornfeldt, in *IEEE International Symposium on Electrical Insulation, 3–6 June, 1990* (IEEE, Piscataway, NJ, 1990), pp. 202–207.
- [18] G. Xie, F. He, X. Liu, L. Si, and D. Guo, *Sci. Rep.* **6**, 25002 (2016).
- [19] D. Das and D. Saintillan, *J. Fluid Mech.* **829**, 127 (2017).
- [20] J. M. Oh, S. H. Ko, and K. H. Kang, *Langmuir* **24**, 8379 (2008).
- [21] N. Benteinitis and S. Krause, *Langmuir* **21**, 6194 (2005).
- [22] J. S. Eow, M. Ghadiri, and A. Sharif, *J. Electrostat.* **51–52**, 463 (2001).
- [23] B. Sarang, P. Basappa, V. Lakdawala, and G. Shivaraj, in *2011 Electrical Insulation Conference (EIC)* (IEEE, Piscataway, NJ, 2011), pp. 377–381.
- [24] O. Fujii, K. Honsali, Y. Mizuno, and K. Naito, *IEEE Trns. Dielectr. Electr. Insul.* **16**, 116 (2009).
- [25] O. Fujii, K. Honsali, Y. Mizuno, and K. Naito, *IEEE Trns. Dielectr. Electr. Insul.* **17**, 566 (2010).
- [26] N. Miljkovic, D. J. Preston, R. Enright, and E. N. Wang, *Nat. Commun.* **4**, 2517 (2013).
- [27] J.-M. Löwe, M. Secklehner, and V. Hinrichsen, in *2017 INSUCON, 13th International Electrical Insulation Conference (INSUCON)* (IEEE, Piscataway, NJ, 2017), pp. 1–7.
- [28] D. Choi, H. Lee, D. J. Im, I. S. Kang, G. Lim, D. S. Kim, and K. H. Kang, *Sci. Rep.* **3**, 2037 (2013).
- [29] L. G. Smith, *Q. J. R. Meteorol. Soc.* **81**, 23 (1955).
- [30] A. M. Selvam, G. K. Manohar, L. T. Khemani, and B. V. R. Murty, *J. Atmos. Sci.* **34**, 1791 (1977).
- [31] R. Gunn and C. Devin, *J. Meteorol. Res.* **10**, 279 (1953).
- [32] L. Rayleigh, *Proc. R. Soc. London* **29**, 71 (1879).
- [33] H. Lamb, *Hydrodynamics* (Cambridge University Press, Cambridge, 1895).
- [34] S. Chandrasekhar, *Proc. London Math. Soc.* **s3-9**, 141 (1959).
- [35] See Supplemental Material at <http://link.aps.org/supplemental/10.1103/PhysRevE.101.023102> for recorded videos of droplet motion for different modes and a table with an overview of all boundary conditions.
- [36] *Springer Handbook of Experimental Fluid Mechanics*, edited by C. Tropea (Springer, Berlin, 2007).
- [37] O. A. Basaran and L. Scriven, *J. Colloid Interface Sci.* **140**, 10 (1990).
- [38] M. Singh, N. Gawande, Y. S. Mayya, and R. Thaokar, *Phys. Fluids* **30**, 122105 (2018).
- [39] J.-M. Löwe and V. Hinrichsen, in *2019 IEEE 20th International Conference on Dielectric Liquids (ICDL)* (IEEE, Piscataway, NJ, 2019), pp. 1–6.
- [40] M. H. Nazemi and V. Hinrichsen, *IEEE Trans. Dielectr. Electr. Insul.* **20**, 443 (2013).
- [41] A. J. B. Milne, B. Defez, M. Cabrerizo-Vilchez, and A. Amirfazli, *Adv. Colloid Interface Sci.* **203**, 22 (2014).
- [42] M. Brandenbourger and S. Dorbolo, *Can. J. Phys.* **92**, 1203 (2014).
- [43] L. Dong, A. Chaudhury, and M. K. Chaudhury, *Eur. Phys. J. E* **21**, 231 (2006).
- [44] X. Noblin, R. Kofman, and F. Celestini, *Phys. Rev. Lett.* **102**, 194504 (2009).
- [45] D. V. Lyubimov, T. P. Lyubimova, and S. V. Shklyaev, *Fluid Dyn.* **39**, 851 (2004).
- [46] M. H. Smith, R. F. Griffiths, and J. Latham, *Q. J. R. Meteorol. Soc.* **97**, 495 (1971).